NASA Technical Memorandum 101984

The Isothermal Fatigue Behavior of a Unidirectional SiC/Ti Composite and the Ti Alloy Matrix

John Gayda, Jr., Timothy P. Gabb, and Alan D. Freed
Lewis Research Center
Cleveland, Ohio

April 1989

NASA

THE ISOTHERMAL FATIGUE BEHAVIOR OF A UNIDIRECTIONAL SiC/Ti COMPOSITE AND THE Ti ALLOY MATRIX

John Gayda, Jr., Timothy P. Gabb, and Alan D. Freed
National Aeronautics and Space Administration
Lewis Research Center
Cleveland, Ohio 44135

SUMMARY

The high temperature fatigue behavior of a metal matrix composite (MMC) consisting of Ti-15V-3Cr-3Al-3Sn (Ti-15-3) matrix reinforced by 33 vol % of continuous unidirectional SiC fibers was experimentally and analytically evaluated. Isothermal MMC fatigue tests with constant amplitude loading parallel to the fiber direction were performed at 300 and 550 °C. Comparative fatigue tests of the Ti-15-3 matrix alloy were also conducted. Composite fatigue behavior and the in-situ stress state of the fiber and matrix were analyzed with a micromechanical model, the Concentric Cylinder Model (CCM).

The cyclic stress-strain response of the composite was stable at 300 °C. However, an increase in cyclic mean strain foreshortened MMC fatigue life at high strain ranges at 550 °C. Fatigue tests of the matrix alloy and CCM analyses indicated this response was associated with stress relaxation of the matrix in the composite.

INTRODUCTION

Currently there is great interest in Ti matrix composites (ref. 1) for aerospace applications at temperatures up to 800 °C. These materials offer increased stiffness and strength at lower densities than monolithic Ti alloys, especially at elevated temperatures (ref. 2). While the potential improvement in monotonic properties is obvious, the effect of fiber reinforcement of Ti matrices with respect to fatigue properties is less certain, especially at elevated temperatures (ref. 3).

The first objective of this paper is to characterize the isothermal fatigue behavior of a unidirectional, SiC/Ti-15-3 composite. To analyze the effect of fiber reinforcement, the fatigue lives of the composite will be compared to that of the Ti-15-3 alloy. This study will be confined to elevated temperature fatigue behavior at 300 and 550 °C; the room temperature fatigue behavior of this system has been characterized by Johnson (ref. 4). Tensile stress-strain behavior will also be examined in this study.

The second objective of this paper is to trace the evolution of the fiber, matrix, and composite stress state during the fatigue test using an analytical approach. The Concentric Cylinder Model, CCM, developed by Ebert and coworkers (refs. 5 and 6) will be employed in this analysis. In essence the CCM approach simulates matrix behavior with a cylindrical shell, which encases a central cylinder that simulates fiber behavior. While this model is limited to loading of unidirectional composites parallel to the fiber direction, it does predict and consider the multiaxial stress state present in all composites, thermally

generated residual stresses, and plasticity effects in the matrix. As Ti alloys creep readily at 550 °C, the CCM approach was modified using a simple "relaxation scheme" to accommodate matrix creep.

MATERIAL AND PROCEDURES

The composite used in this study had a Ti-15V-3Cr-3Al-3Sn alloy matrix (Ti-15-3), strengthened by 33±0.5 vol % of continuous SiC fiber, SCS-6. A detailed description of the composite microstructure is contained elsewhere (ref. 7). All composite specimens used in this study were obtained from a single, eight-ply, unidirectional panel manufactured by Textron Specialty Materials Division. The composite panel was 30 by 30 by 0.21 cm. Textron also fabricated a Ti-15-3 alloy plate without fibers, 30 by 30 by 1.0 cm, using the same Ti-15-3 foil and consolidation techniques employed in composite production. The 1.0 cm dimension was desired to facilitate tension/compression testing of the matrix alloy.

Flat composite test specimens, shown in figure 1, were machined from the composite panel using a two step machining process. A slightly oversized specimen was first machined with a wire EDM procedure and then diamond ground to remove damaged material and obtain the desired dimensions. Cylindrical test specimens of the matrix alloy were ground to the dimensions shown in figure 2. This specimen design can accommodate the tension/compression loading which can arise in high temperature, strain-controlled fatigue tests. After machining, the composite and the matrix alloy specimens were both heat treated at 593 °C for 24 hr in an argon atmosphere to stabilize the microstructure and therefore the properties of the matrix.

Isothermal fatigue test on the composite were run using a load-controlled servohydraulic test system equipped with hydraulic wedge grips. A triangular waveform was employed with a minimum load of zero to prevent compressive loading of the thin specimens. The loading rate was adjusted to give a relatively constant strain rate of 0.001 sec^{-1}. This was possible as the composite response was essentially linear. In all tests, the fiber direction and the loading axis were parallel within 1°. Axial strain measurements were made with a high temperature extensometer having a 12.5 mm gage length attached to the edge of the specimen. Direct induction heating was employed in all tests and specimen temperature was controlled using an infrared pyrometer. A temperature gradient of less than 10 °C was maintained within the gage length of the specimen.

Isothermal fatigue tests on the matrix alloy were run using a strain-controlled servohydraulic test system. While strain-controlled testing of the matrix alloy may seem inappropriate as load-control was employed for the composite, this choice is not irrational, as matrix deformation in the composite is very much a strain-controlled situation resulting from the elastic response of the fibers. A triangular waveform and a strain rate of 0.001 sec^{-1} were usually employed. However, in the lowest strain range test at 300 °C a strain rate of 0.01 sec^{-1} was employed to generate life data more rapidly. In all tests, a zero/tension strain ratio was enforced to simulate the matrix behavior in the composite. A three-zone electric furnace was used for heating. Specimen temperature was controlled using a type K thermocouple. Axial strain measurements were made using a high temperature extensometer of 12.5 mm gage length.

For both composite and matrix alloy, stress versus strain hysteresis loops were periodically recorded using an x-y recorder. In addition, stress versus time and strain versus time data were continually recorded with a two-pen strip chart.

RESULTS AND DISCUSSION

Tensile Behavior

Typical tensile stress-strain curves for the matrix alloy are presented in figure 3. As expected, the strength and moduli decrease as the temperature increases. The elongation increases from 13 percent at 300 °C to 42 percent at 550 °C.

Typical tensile stress-strain curves for the composite are presented in figure 4. While the moduli and the strength of the composite decrease with increasing temperature, the strain to failure shows no significant temperature dependence. The composite failure strain apparently is governed by the failure strain of the fibers, which is relatively constant over this temperature range (manufacturer's data). Using the rule of mixtures and elastic moduli measurements for the composite and matrix alloy, the average fiber modulus, E, is computed to be 370 GPa at 300 °C and 350 GPa at 550 °C. A similar calculation employing the tensile stress-strain curves of the composite and matrix alloy indicates average fiber strengths, S_u of 2800 MPa at 300 °C and 2700 MPa at 550 °C. These calculated properties have lower values than those reported (manufacturer's data) for virgin fibers, $E > 400$ GPa and $S_u > 3500$ MPa, implying fiber degradation has occurred during consolidation, machining, and/or heat treating.

Fatigue Behavior of Matrix Alloy

The results of fatigue tests on the matrix alloy are summarized in table I, and the isothermal total strain range versus fatigue life curves are presented in figure 5. The upper and lower strain ranges examined were chosen to coincide with that of the composite. As seen in the figure, the fatigue life at 550 °C is superior to that at 300 °C. This is probably due to a difference in mean stress. At 300 °C there is little stress relaxation, and a tensile mean stress is maintained throughout the test. However, at 550 °C, the cyclic mean stress approaches zero at a rapid rate, as shown in figure 6. Hence, the 550 °C fatigue tests develop a stress ratio ($R_\sigma = \sigma_{min}/\sigma_{max}$) of -1 by half life, while the 300 °C fatigue tests maintain a zero stress ratio for the most part. Unlike mean stress, the stress range did not vary significantly in these tests. As seen in table I, the stress range at cycle one, 100, and half life are essentially unchanged.

At either temperature, the low strain life data in figure 5 are plotted as runouts. All three of these tests were terminated by a shear-type thread failure. Past experience with this specimen design (ref. 8) has never produced this type of failure, suggesting that the in-plane shear strength of the matrix alloy plate is relatively low. This effect may be related to the strength of the foil-foil interfaces in the matrix alloy.

Fatigue Behavior of the Composite

The results of fatigue tests on the composite are summarized in table II. As the fatigue data on the composite were generated using a load-controlled test system, a stress based comparison of the composite and the matrix alloy will be presented first (fig. 7). At 300 °C the fatigue life of the composite is more than 10 times greater than that of the matrix alloy at a stress range of 700 MPa. Note that the mean stress ratio, R_σ, for either material is essentially zero at 300 °C. At 550 °C, the composite still has a life which is greater than that of the matrix alloy at this stress level. However, the difference is smaller than that observed at 300 °C. This may be due in large part to the difference in stress ratios of the composite and the matrix alloy at 550 °C. The composite stress ratio is held at zero, but as previously stated, the stress ratio of the matrix alloy rapidly decreases from zero to -1 despite having held the strain ratio at zero. An analysis of the change in the stress ratio within the matrix of the composite will be discussed later.

At stresses below 1000 MPa, the 300 and 550 °C fatigue life lines of the composite have similar slopes, but the 300 °C life is approximately three times longer than the 550 °C life on a stress basis. The longer life of the composite at 300 °C is to be expected, as the strength of the composite is higher at this temperature, due in large part to the higher strength of the Ti matrix.

At stresses above about 1000 MPa, the 550 °C fatigue life of the composite is greatly foreshortened. At a stress of 1095 MPa, the fatigue life at 550 °C was only 10 cycles compared to a life of 3000 cycles at 300 °C. This life reduction at high stresses is apparently related to the inability of the matrix to maintain a mean stress at 550 °C, i.e., the matrix creeps. For all stress ranges, the composite shows a pronounced increase in mean strain (due to tensile creep of the matrix) during cycling at 550 °C, which was not found in tests at 300 °C. Figure 8 compares the change in mean strain during 300 and 550 °C fatigue tests at comparable stress ranges. In these load-controlled tests the inability of the matrix to support a mean stress at 550 °C, as previously shown in figure 6, would produce the observed change in mean strain of the composite. The stress which is shed by the matrix is transferred to the fibers, and this load transfer apparently shortens life at high stresses, as the tensile strength of the weaker fibers is exceeded. Failure of the weaker fibers increases the stress on the adjacent fibers, thereby causing failure of these fibers and so on until the entire specimen fails. At lower stresses the load transfer and subsequent increase in mean strain still occurs at 550 °C, but the peak fiber stress is apparently not sufficient to immediately fail the weaker fibers. As premature tensile failure of fibers does not occur, a longer fatigue life results.

While a stress-based comparison of the fatigue lives of the composite and the matrix alloy is important from certain application standpoints, to understand fatigue failure, it is probably more instructive to compare fatigue life on a strain basis. The fatigue lives of the composite and matrix alloy are plotted against total strain range at half life in figure 9. At 300 and 550 °C the life of the composite is less than that of the matrix alloy, although the difference is much smaller at 300 °C. Note that the 300 and 550 °C lives of the composite converge at low strains. This is reasonable, as a strain-based comparison tends to normalize temperature-induced differences in moduli and strength which often produce life differences when fatigue life is viewed on a stress basis. At large strains the difference in composite fatigue

life (300 versus 550 °C) observed on a stress basis is still evident. In fact, the difference is even more apparent, as a strain range of 0.8 percent gives a life of 900 cycles at 300 °C while a strain range of 0.65 percent gives a life of only 10 cycles at 550 °C.

On a strain basis, the life deficit of the composite relative to that of the matrix alloy suggests that the matrix, in and by itself, does not control life. Nor is it expected that the fiber in and by itself controls life. To examine these points in more detail, the evolution of the fiber, matrix, and composite stress states will now be analyzed using the CCM approach outlined in the introduction of this paper.

Concentric Cylinder Model

The CCM can be used to analyze unidirectional composite behavior under thermal and mechanical loading. In this model, the composite continuum is simulated by two cylinders (fig. 10). For fiber volume fractions less than 50 percent the central cylinder is the fiber simulator and the outer cylinder is the matrix simulator. Setting the radius of the matrix simulator at one, the radius of the fiber simulator is dictated by the volume fraction. For a 33 vol % fiber fraction the radius of the fiber simulator is 0.57.

The axial (S_z), radial (S_r), and tangential (S_t) stress distributions for this geometry are essentially that of a thick wall pressure vessel. In both problems, the radial displacement, u, from which all strains and stresses are computed, is governed by:

$$u = Ar + \frac{B}{r} \tag{1}$$

where r is the radial coordinate and A and B are constants which for the pressure vessel problem are dependent on the fluid pressure. In the CCM problem, the imposition of a force balance in the axial direction and the inclusion of a thermal strain term in Hooke's law generate the "fluid pressure." A further difference, which is obvious, is that the central cylinder takes on properties of a solid not a fluid.

Deformation plasticity in the matrix simulator can be accommodated by adopting an incremental solution scheme and replacing the elastic constants, E and V, in Hooke's law with the appropriate plastic constants when the matrix flows. To determine the onset of plastic flow, the von Mises yield criterion was employed using the three principal stresses, S_z, S_r, and S_t. As S_r and S_t are functions of r, one is forced to choose a location at which matrix properties are evaluated. In this study, $r = 0.82$ was selected, as this location bisects the matrix simulator into equal parts on an area basis.

The need to simulate creep of the matrix is of paramount importance at these temperatures. At this time, a rigorous, theoretical analysis of this problem will not be attempted; instead a simple "relaxation scheme" will be employed. Essentially this is a two part procedure. First the matrix stress distribution is allowed to relax for a given period of time. Computationally, this is achieved by allowing all three principal stresses to decay at a rate which is determined by the initial magnitude of that component of stress at a given location. Second, to maintain equilibrium, the fiber stress distribution

must be altered. In the axial direction, this is achieved by adjusting the fiber stress, S_z, to counteract the decrease in the matrix stress, S_z, such that the composite stress is unchanged. In the transverse directions, the fiber stresses, S_r and S_t, are set equal to the matrix stress, S_r, at the interface. The axial strain of the composite, e, will also change and it can be approximated by:

$$e_{new} = e_{old} + \frac{(dS_z - 2V_f\, dS_r)}{E_f} \qquad (2)$$

where dS_z and dS_r are the change in the axial and radial fiber stress respectively and E_f and V_f are the modulus and Poisson ratio of the fiber.

As an incremental approach is needed for CCM problems involving matrix plasticity or creep, a computer-oriented formulation of the CCM is highly desirable. The actual computer codes used in this investigation, TCCM and MCCM, were written in BASIC and are listed in the appendix. TCCM was used to track the evolution of residual stresses in the fiber and matrix on cooling and heating, while MCCM was used to track the fiber, matrix, and composite stresses during the fatigue tests. In both codes, a relaxation subroutine was executed using an appropriate time increment, following each incremental change in temperature (TCCM) or strain (MCCM). The temperature and strain increments are, from the standpoint of the analysis, instantaneous.

The physical and mechanical properties of the fiber and matrix used in these analyses are also listed in the appendix. While the stress-strain behavior of the fiber is assumed to be linear and temperature insensitive, a bilinear, temperature dependent stress-strain curve is used to model matrix behavior. Both of these assumptions are fair approximations of actual tensile data for the fiber and matrix. An empirical fit of stress relaxation data for the matrix alloy, figure 11, was used to predict time dependent composite behavior at 550 °C. As negligible relaxation was observed at 300 °C, the analyses ignored the effect of creep at this temperature. Linear interpolation was used to predict relaxation rates at temperatures between these two extremes.

Thermally Generated Residual Stresses

Before one can track the fiber, matrix, and composite stresses in fatigue tests, an initial estimate of the residual stress distribution is needed. Assuming the composite is stress free at the consolidation temperature, on cooling to room temperature a tensile stress state will develop in the matrix, as the thermal expansion coefficient of the matrix is almost twice that of the fiber. The fiber must in turn develop a compressive stress state to counteract the matrix stresses. When the composite is aged at 593 °C for 24 hr, the residual stresses are greatly reduced by the rise in temperature and matrix creep. In fact, the residual stresses in the composite are likely to be very small near the end of the aging heat treatment.

An upper bound for these stresses can be obtained by using the TCCM code and ignoring any relaxation effects up to the beginning of the 24 hr age. More specifically, the TCCM code was run assuming the following thermal history.

The composite is assumed initially stress free at 1000 °C. The composite is then cooled to room temperature instantaneously. Then, the composite is heated to 593 °C instantaneously and held at 593 °C for 24 hr. The resulting residual stress distributions at room temperature, at 593 °C at the beginning of the age, and 593 °C near the end of the age, are presented in figure 12. While the peak stresses in the composite are quite large at 20 °C after cool down from 1000 °C, near the end of the 593 °C age, the peak stresses are less than 15 MPa in the matrix and about -30 MPa in the fiber. Recalling that these are upper bounds, it is reasonable to assume the composite is stress free at 593 °C near the end of the age. Although the residual stresses are negligible, this does not mean there is no damage at this point in time. The large tensile stresses encountered at room temperature could produce cracking. From a stress standpoint, radial cracking at the fiber matrix interface is most likely since the largest tensile stress, S_t, is found at this location. Formation of cracks will, of course, depend on other factors also, such as the strength of the matrix and interface.

After aging, the composite is cooled to room temperature and subsequently reheated to the test temperature. As before, a tensile stress state is produced in the matrix as the composite is cooled from 593 °C to room temperature. When the composite is heated to the testing temperature, the magnitude of the residual stresses is reduced. Assuming a 5 °C/sec heating and cooling rate, the TCCM code was used to track the residual stresses. The final stress distributions at the appropriate test temperatures are presented in figure 13. At 300 °C the axial stress level in the matrix is 83 MPa, while that of the fiber is -165 MPa. The transverse stresses generated by temperature changes are also significant. In fact, the largest matrix stress is found in the tangential stress distribution, which peaks at 105 MPa at the fiber-matrix interface. At 550 °C the residual stress distribution of the composite is nearly zero in all directions, due in large part to the increase in temperature.

Fatigue Analysis

Analysis of the tensile tests and fatigue cycles were run using the MCCM code and the starting residual stress distributions obtained above.

At 300 °C, the predicted composite behavior on loading in a tensile test to 0.85 percent strain, the experimentally measured fracture strain, is plotted in figure 14. The experimental stress strain data is also shown for comparative purposes. Composite behavior is totally elastic up to 0.65 percent strain. At this point, the axial stress in the matrix and fiber is 724 and 2096 MPa respectively. Further, the combination of axial and transverse stresses in the matrix satisfy the von Mises yielding criterion, and strains above 0.65 percent produce plastic flow in the matrix. As a result, the increase in matrix stresses is limited, and at the failure strain, 0.85 percent, the matrix stress, S_z, increases by only 34 MPa to 758 MPa. In comparison, the fiber stress, S_z, has increased some 654 MPa to 2750 MPa. Unlike thermal strains, the application of mechanical strains does not produce dramatic changes in the transverse stress distribution. At 0.85 percent strain the transverse stresses in the fiber are still only -84 MPa. The transverse stress distribution in the matrix also show proportionately small increases.

The computed axial stress histories for the fiber, matrix, and composite are summarized in figure 15 for fatigue cycles at 300 °C. The analysis of the

300 °C fatigue cycle at low stresses is simple as the stresses in all constituents remain elastic, as suggested from the experimental hysteresis loops. For example, in a test where the composite stress is cycled between 0 and 710 MPa, the axial stress of the matrix is found to cycle between 83 and 470 MPa, while that of the fiber is found to cycle between -165 and 1205 MPa. The minimum stresses of the fiber and matrix are nonzero because residual stresses are present at the start of the test. Further, the stress amplitudes generated in cycle one remain constant in subsequent cycles. These results change at higher stress ranges where the flow stress of the matrix is exceeded. For a stress range of 1345 MPa, the initial cycle produces an inelastic strain of 0.043 percent as matrix flow occurs on loading but totally elastic behavior is observed on unloading. Subsequent cycles are totally elastic and retrace the unloading line for cycle one, this is consistent with experimental measurements. Flow of the matrix alters the distribution of stress between fiber and matrix. The fiber stress, S_Z, starts at -165 MPa rises to a peak of 2580 MPa at maximum load and then drops to -15 MPa at zero load. The matrix stress starts at 83 MPa rises to a peak of 750 MPa at maximum load and then drops to 8 MPa at zero load. In subsequent cycles the fiber and matrix stresses continue to cycle between these altered values. As was the case for the tensile analysis, the change in the transverse stress distribution is quite small.

At 550 °C, the predicted composite behavior on loading in a tensile test to 0.85 percent, the experimentally measured fracture strain, is plotted in figure 16. The experimental stress strain data is also shown for comparative purposes. Unlike the 300 °C tensile curve, a small nonlinear response associated with matrix creep is observed before the onset of matrix flow. As the transverse stresses are very small at 550 °C, matrix flow occurs when the axial stress in the matrix reaches 450 MPa, the assumed yield strength of the matrix. Continued loading out to the fracture strain increases the matrix stress only 33 MPa to 483 MPa, while the fiber stress increases some 696 MPa, from a low of 2200 MPa at the onset of matrix flow to a high of 2896 MPa at failure.

The fatigue analysis at 550 °C is much more complicated than that at 300 °C due to the nonlinear stress-strain behavior and is illustrated in figure 17. At a composite stress range of only 655 MPa the initial cycle produces a tensile inelastic strain of 0.02 percent. At this stress range, the inelastic strain is produced by matrix creep not matrix plasticity. Subsequent cycles show an inelastic strain of decreasing magnitude. As a result the mean strain level of the composite increases as shown in figure 17(a). By cycle 100 the stress-strain behavior of the composite becomes linear and there is no further increase in mean strain. This is in good agreement with experimental observations. The change in the axial stress level of the fiber and matrix during this period is plotted in figure 17(b). As seen here, the maximum fiber stress rises while the maximum matrix stress drops in the first 100 cycles. For a stress range of 1069 MPa the fatigue analysis is even more complex as plastic flow of the matrix occurs during the initial loading. The combination of matrix plasticity and creep produce an inelastic strain of 0.04 percent on unloading. Although nonlinear behavior producing inelastic strain is observed in subsequent cycles, the nonlinearity is associated with matrix creep, not matrix plasticity. As before, the magnitude of this inelastic strain diminishes with each successive cycles, and by cycle 100 composite stress-strain behavior is essentially linear, as observed experimentally. The mean strain level of the composite is shown in figure 18 along with the fiber stress and the matrix stress. Although larger, the change in mean strain, fiber stress, and matrix stress, is very similar to that observed at the lower stress range (fig. 17).

The above calculations largely confirm the validity of the strain-based fatigue life comparison between the composite and the matrix alloy presented in figure 9. The CCM analysis shows that the matrix stress state in the composite approximates the zero-tension stress state of the matrix alloy at 300 °C, and at 550 °C the same can be said of the tension-compression stress state of the matrix alloy. However, the matrix stress state in the composite only approaches a uniaxial condition, as small but nonnegligible transverse stresses exist in the composite. Further, at 300 °C the axial stress of the matrix within the composite only approaches the zero-tension condition of the matrix alloy fatigue tests as the initial residual stress distribution favors a tension-tension condition at lower stress ranges (fig. 15).

As previously stated, the fatigue life of the composite is less than that of the matrix alloy on a stain basis (fig. 9). At 300 °C the life difference is about a factor of five, and at 550° and stresses less than 1000 MPa the life difference is about two orders of magnitude. These observations suggest that the matrix does not control the fatigue life of the composite in and by itself. Further, as fatigue-related failures in ceramics are rare, a fiber dominated failure scenario would also seem unlikely at low stress ranges. Thus, one might conclude that a complex failure process involving the matrix, the fibers, and the interface is life limiting. In fact, metallographic and fractographic evidence for a fatigue failure process of crack initiation at the fiber-matrix interface followed by crack propagation through the matrix is presented in a publication submitted to "Journal of Composite Materials". The details of this process are not well understood at this time, and it would appear that this is an important area requiring additional research. Key factors to be considered include the role of fiber flaws on interface/matrix crack initiation, the effect of fibers on matrix crack propagation, interaction between individual cracks, as well as multiaxiality and residual stress effects.

At 550 °C and stresses greater than 1000 MPa, the life of the composite appears to be controlled by the fibers. The CCM analysis has shown that the fiber stress approaches the fibers' ultimate strength quite rapidly (fig. 18). Although the kinetics of this process are controlled by the creep behavior of the matrix alloy, ultimate failure probably occurs when the tensile strength of weaker fibers is exceeded.

CONCLUSIONS

The isothermal fatigue behavior of a unidirectional SiC/Ti-15-3 composite and the Ti-15-3 matrix alloy were studied at 300 and 550 °C. A summary of the findings follow:

1. The cyclic stress-strain response of the composite and the matrix alloy was relatively stable at 300 °C. However, at 550 °C, an initial increase in mean strain was observed during the first 100 cycles for load-controlled, composite fatigue tests. For strain-controlled matrix alloy fatigue tests, the mean stress rapidly approached zero at 550 °C.

2. Although the fatigue life of the composite exceeded that of the matrix alloy on a stress basis, the fatigue life of the matrix alloy exceeded that of the composite on a strain basis.

3. The Concentric Cylinder Model (CCM) thermal stress analysis has shown that a large and potentially damaging multiaxial stress field is generated in the composite upon cooling down from the fabrication temperature. These stresses are eliminated by matrix creep during the 593 °C age, but are partially regenerated on cooling. The thermally generated residual stress field is negligible in both constituents at 550 °C, but a significant tensile stress field exists in the matrix counterbalanced by a compressive stress field in the fiber at 300 °C.

4. The CCM stress analysis of the fatigue cycles has shown that the stress response in the fiber and matrix is largely uniaxial as transverse stresses show little change. Along the fiber direction, the mean stress in the matrix and fiber is relatively stable at 300 °C; however, at 550 °C, matrix creep allows the mean stress in the matrix to approach zero, while that in the fiber must rise to maintain the axial force balance.

In conclusion, the experimental data and the CCM stress analysis suggest that the matrix does not control the fatigue life of the composite in and by itself. At 550 °C and high stress ranges, a fiber-dominated failure scenario is plausible due to the gradual rise in fiber stress. At 300 °C and lower stress ranges at 550 °C, an interface crack initiation/matrix crack propagation mechanism is thought to limit fatigue life of the composite.

REFERENCES

1. Froes, F.H.: Space-age Metals Technology. J. Met., vol. 40, no. 11, Nov. 1988, pp. 12-16.

2. Brindley, P.K.; Bartolotta, P.A.; and Klima, S.J.: Investigation of a SiC/Ti-24Al-11Nb Composite. NASA TM 100956, 1988.

3. Bhatt, R.T.; and Grimes, H.H.: Fatigue Behavior of SiC Reinforced Titanium Composites. Fatigue of Fibrous Composite Materials. Am. Soc. Test. Mater. Spec. Tech. Publ. (723), 1981, pp. 274-290.

4. Johnson, W.J.: Fatigue Testing and Damage Development in Continuous Fiber Reinforced Metal Matrix Composites. NASA TM-100628, 1988.

5. Ebert, L.J.; and Gadd, J.D.: A Mathematical Model for Mechanical Behavior of Interfaces in Composite Materials. Fiber Composite Materials. American Society for Metals, 1965, pp. 89-113.

6. Hecker, S.S.; Hamilton, C.H.; and Ebert, L.J.: Elastic-plastic analysis: A Simplified Approach, Scr. Metall., vol. 3, no. 11, 1969, pp. 793-798.

7. Lerch, B.A.; Hull, D.R.; and Leonhardt, T.A.: As-received Microstructure of a SiC/Ti-15-3 Composites. NASA TM-100938, 1988.

8. Gabb, T.P.; Gayda, J.; and Miner, R.V.: Orientation and Temperature Dependence of Some Mechanical Properties of the Single-crystal Nickel-base Superalloy Rene N4: Part II. Low Cycle Fatigue Behavior. Met. Trans. A, vol. 17, no. 3, Mar. 1986, pp. 497-505.

APPENDIX

The properties of the fiber and matrix used in the CCM analysis are present below. Note that all fiber properties are taken to be independent of temperature.

Property	Fiber	Matrix
Expansion coefficient Poisson's ratio	4.9×10^{-6} C^{-1} 0.25	9.0×10^{-6} C^{-1} 0.35
300 °C Modulus 550 °C Modulus	350 GPa 350 GPa	100 GPa 75 GPa
300 °C Yield point 550 °C Yield point	---------- ----------	700 MPa 450 MPa

Upon yielding the tangent, moduli of the matrix was taken to be 15 GPa at either temperature. A listing of the two BASIC codes used in this analysis TCCM and MCCM, are presented on the following pages. Both codes were run on an IBM AT computer using the GW-BASIC interpreter (version 3.20). Note that the constants in these codes are expressed in English units (KSI and °F), and in MCCM, the mechanical properties shown are those for a 550 °C analysis.

```
10 REM THERMAL/RELAXATION CONCENTRIC CYLINDER MODEL (TCCM)
20 REM INPUT RESIDUAL STRESS DISTRIBUTION
30 PI=3.14159
40 OPEN "I",#1,"RESID"
50 FOR I=1 TO 5
60 INPUT #1,RSZM(I),RSRM(I),RSTM(I)
70 NEXT I
80 INPUT #1,RSZF,RSRF,RSTF,TEZ,TEMP,TIM,HO
90 CLOSE #1
100 PRINT "PREVIOUS TEMPERATURE(F) WAS";TEMP
110 LPRINT "PREVIOUS TEMPERATURE(F) WAS";TEMP
120 REM INPUT PROPERTIES OF FIBER(F) AND MATRIX(M)
130 REM TEMPERATURE INDEPENDENT ELASTIC CONSTANTS
140 EF=50000!:VF=.25:VM=.35
150 REM RADIAL LOCATION OF BOUNDARIES
160 RF=.57:RM=1!
170 RP(1)=RF
180 RP(2)=.7
190 RP(3)=.82
200 RP(4)=.91
210 RP(5)=RM
220 REM COEFFICIENTS OF EXPANSION
230 AF=.0000027:AM=.000005
240 REM INPUT CHANGE IN TEMPERATURE(DT)
250 INPUT "DT (ENTER 0 TO STOP)";DT
260 TEMP=TEMP+DT/2!
270 IF DT=0 THEN 2280
280 REM GENERATE SYSTEM OF EQUATIONS FOR THERMAL PROBLEM [A]x[X]=[B]
290 REM UNKNOWNS [X] ARE C1F, C1M, C2M, AND EZ (C2F=0)
300 REM WHERE THE RADIAL DISPLACEMENT U=C1*R+C2/R^2 AND EZ=AXIAL STRAIN
310 REM STIFFNESS CONSTANTS FOR PLANE STRAIN (EZ IS CONSTANT)
320 REM CHECK FOR FLOW IN MATRIX
330 EFS=(RSZM(3)-RSRM(3))^2+(RSRM(3)-RSTM(3))^2
340 EFS=.707*(EFS+(RSTM(3)-RSZM(3))^2)^.5
350 YS=152.5-(35/400)*TEMP+HO
360 IF YS<10 THEN YS=10
370 IF EFS<YS THEN FLOW=0:GOTO 450
380 PRINT "MATRIX FLOW DETECTED! EFS, YS=";EFS;YS
390 REM FLOW=0 ELASTIC BEHAVIOR
400 REM FLOW=1 ELASTIC BEHAVIOR WITH PRIOR HARDENING
410 REM FLOW=2 PLASTIC BEHAVIOR WITH PRIOR HARDENING
420 INPUT "FLOW(0=E, 1=E&H, 2=P&H)";FLOW
430 IF FLOW>0 THEN HO=HO+EFS-YS
440 PRINT "EFS,YS=";EFS;YS
450 REM CALCULATE MATRIX STIFFNESS CONSTANTS AEM & AVM
460 IF FLOW=2 THEN AEM=2300:AVM=.49
470 IF FLOW<2 THEN AEM=18500-(3000/400)*TEMP:AVM=VM
480 IF AEM>14000 THEN AEM=14000
490 PRINT "AEM, AVM=";AEM,AVM
500 K1F=EF*(1-VF)/((1+VF)*(1-2*VF))
```

```
510 K1M=AEM*(1-AVM)/((1+AVM)*(1-2*AVM))
520 K2F=VF*K1F/(1-VF)
530 K2M=AVM*K1M/(1-AVM)
540 KTF=K1F*(1+VF)/(1-VF)
550 KTM=K1M*(1+AVM)/(1-AVM)
560 REM GENERATE [A] MATRIX
570 REM UM=UF AT R=RF IS THE BASIS OF EQUATION 1
580 A(1,1)=RF
590 A(1,2)=-RF
600 A(1,3)=-1/RF
610 A(1,4)=0
620 REM THE RADIAL STRESS SRM=0 AT R=RM IS THE BASIS OF EQUATION 2
630 A(2,1)=0
640 A(2,2)=K1M+K2M
650 A(2,3)=(K2M-K1M)/RM^2
660 A(2,4)=K2M
670 REM SRM=SRF AT R=RF IS THE BASIS OF EQUATION 3
680 A(3,1)=-K1F-K2F
690 A(3,2)=K1M+K2M
700 A(3,3)=(K2M-K1M)/RF^2
710 A(3,4)=K2M-K2F
720 REM BALANCE OF FORCES SZM+SZF=0 IS THE BASIS OF EQUATION 4
730 A(4,1)=2*RF^2*K2F
740 A(4,2)=2*(RM^2-RF^2)*K2M
750 A(4,3)=0
760 A(4,4)=RM^2*K1M-RF^2*K1M+RF^2*K1F
770 REM GENERATE [B] MATRIX
780 B(1)=0
790 B(2)=KTM*AM*DT
800 B(3)=(AM*KTM-AF*KTF)*DT
810 B(4)=(KTF*AF*RF^2+KTM*AM*(RM^2-RF^2))*DT
820 REM TRIANGULARIZE SYSTEM OF LINEAR EQUATIONS
830 FOR I=1 TO 3
840 FOR J=I+1 TO 4
850 XX=A(J,I)/A(I,I)
860 FOR K=I+1 TO 4
870 A(J,K)=A(J,K)-A(I,K)*XX
880 NEXT K
890 B(J)=B(J)-B(I)*XX
900 NEXT J
910 NEXT I
920 REM SOLVE BY BACKWARD SUBSTITUTION
930 X(4)=B(4)/A(4,4)
940 FOR I=3 TO 1 STEP -1
950 DUM=0
960 FOR J=I+1 TO 4
970 DUM=DUM+A(I,J)*X(J)
980 NEXT J
990 X(I)=(B(I)-DUM)/A(I,I)
1000 NEXT I
```

```
1010 REM CALCULATE STRESSES(Si,j) AND STRAINS(Ei,j)
1020 REM WHERE i IS A PRINCIPAL DIRECTION AND j IS A COMPONENT
1030 REM ER=C1-C2/R^2 AND ET=U/R=C1+C2/R^2
1040 C1F=X(1)
1050 C1M=X(2)
1060 C2M=X(3)
1070 EZ=X(4)
1080 REM CALCULATE MATRIX STRAINS AND STRESSES
1090 FOR I=1 TO 5
1100 R=RP(I)
1110 ERM=C1M-C2M/R^2
1120 ETM=C1M+C2M/R^2
1130 EZM=EZ
1140 SRM=K1M*ERM+K2M*ETM+K2M*EZM-KTM*AM*DT
1150 STM=K1M*ETM+K2M*ERM+K2M*EZM-KTM*AM*DT
1160 SZM=K1M*EZM+K2M*ERM+K2M*ETM-KTM*AM*DT
1170 RSZM(I)=RSZM(I)+SZM
1180 RSRM(I)=RSRM(I)+SRM
1190 RSTM(I)=RSTM(I)+STM
1200 PRINT "SZ, SR, ST ARE AT R=";
1210 PRINT USING "#.##";R
1220 PRINT USING " ##.##^^^^";RSZM(I),RSRM(I),RSTM(I)
1230 NEXT I
1240 REM CALCULATE FIBER STRAINS AND STRESSES
1250 R=RF
1260 ERF=C1F
1270 ETF=C1F
1280 EZF=EZ
1290 SRF=K1F*ERF+K2F*ETF+K2F*EZF-KTF*AF*DT
1300 STF=K1F*ETF+K2F*ERF+K2F*EZF-KTF*AF*DT
1310 SZF=K1F*EZF+K2F*ERF+K2F*ETF-KTF*AF*DT
1320 RSZF=RSZF+SZF
1330 RSRF=RSRF+SRF
1340 RSTF=RSTF+STF
1350 TEZ=TEZ+EZ
1360 PRINT "SZ, SR, ST IN FIBER"
1370 PRINT USING " ##.##^^^^";RSZF,RSRF,RSTF
1380 REM OUTPUT TEMPERATURE, STRAIN, AND STRESS
1390 ZLOAD=PI*RF^2*RSZF
1400 FOR I=1 TO 4
1410 AVGS=(RSZM(I)+RSZM(I+1))/2
1420 AVGL=AVGS*PI*(RP(I+1)^2-RP(I)^2)
1430 ZLOAD=ZLOAD+AVGL
1440 NEXT I
1450 PRINT "COMPOSITE TEMPERATURE, STRAIN, AND STRESS"
1460 PRINT TEMP+DT/2!;
1470 PRINT USING " ##.##^^^^";TEZ,ZLOAD/(PI*RM^2)
1480 LPRINT "TIME, TEMP=";TIM;TEMP+DT/2
1490 LPRINT "COMPOSITE STRAIN, STRESS=";
1500 LPRINT USING " ##.##^^^^";TEZ,ZLOAD/(PI*RM^2)
```

```
1510 LPRINT "Z,R,T FIBER STRESSES=";
1520 LPRINT USING " ##.##^^^^";RSZF,RSRF,RSTF
1530 LPRINT "Z,R,T MATRIX STRESSES=";
1540 LPRINT USING " ##.##^^^^";RSZM(3),RSRM(3),RSTM(3)
1550 REM START OF RELAXATION SUBROUTINE
1560 REM CALCULATE EXTERNAL LOAD
1570 PI=3.14159
1580 ELOAD=PI*RF^2*RSZF
1590 FOR I=1 TO 4
1600 AVGS=(RSZM(I)+RSZM(I+1))/2
1610 AVGL=AVGS*PI*(RP(I+1)^2-RP(I)^2)
1620 ELOAD=ELOAD+AVGL
1630 NEXT I
1640 REM INPUT TIME INCREMENT
1650 INPUT "TIME INCREMENT (0 TO STOP)";TI
1660 IF TI=0 THEN TEMP=TEMP+DT/2:GOTO 250
1670 TI=TI-1
1680 IF TI<0 THEN GOTO 2180
1690 TIM=TIM+1
1700 REM ADJUST MATRIX STRESSES
1710 FOR I=1 TO 5
1720 S=RSZM(I)
1730 GOSUB 2010
1740 RSZM(I)=S
1750 S=RSRM(I)
1760 GOSUB 2010
1770 RSRM(I)=S
1780 S=RSTM(I)
1790 GOSUB 2010
1800 RSTM(I)=S
1810 NEXT I
1820 REM ADJUST TRANSVERSE FIBER STRESSES
1830 RSRFO=RSRF
1840 RSRF=RSRM(1)
1850 RSTF=RSRF
1860 REM CALCULATE LOAD CARRIED BY FIBER
1870 MLOAD=0
1880 FOR I=1 TO 4
1890 AVGS=(RSZM(I)+RSZM(I+1))/2
1900 AVGL=AVGS*PI*(RP(I+1)^2-RP(I)^2)
1910 MLOAD=MLOAD+AVGL
1920 NEXT I
1930 FLOAD=ELOAD-MLOAD
1940 RSZFO=RSZF
1950 REM ADJUST Z STRESS OF FIBER
1960 RSZF=FLOAD/(PI*RF^2)
1970 REM CALCULATE COMPOSITE STRAIN
1980 EZ=((RSZF-RSZFO)-2*VF*(RSRF-RSRFO))/EF
1990 TEZ=TEZ+EZ
2000 GOTO 2080
```

```
2010 REM RELAXATION PROCEDURE (1 SECOND RELAXATION)
2020 IF TEMP<600 THEN DS=0:GOTO 2060
2030 IF ABS(S)>26.5 THEN DS=ABS(S)/50 ELSE DS=3.76E-07*ABS(S)^4.32
2040 DS=DS*(TEMP-600)/(1000-600)
2050 IF S<0 THEN DS=-DS
2060 S=S-DS
2070 RETURN
2080 REM OUTPUT STRESSES, TEMPERATURE, AND AXIAL STRAIN
2090 PRINT "TIME=";TIM;"STRAIN=";TEZ
2100 IF TI>0 THEN GOTO 1670
2110 PRINT "FIBER STRESSES(Z,R,T)=";RSZF;RSRF;RSTF
2120 FOR I=1 TO 5
2130 PRINT "MATRIX RADIAL LOCATION=";RP(I)
2140 PRINT USING "  ###.##";RSZM(I),RSRM(I),RSTM(I)
2150 NEXT I
2160 TEMP=TEMP+DT/2!
2170 PRINT "TIME=";TIM;"TEMP=";TEMP
2180 REM END OF RELAXATION SUBROUTINE
2190 LPRINT "TIME, TEMP=";TIM;TEMP
2200 LPRINT "COMPOSITE STRAIN, STRESS=";
2210 LPRINT USING " ##.##^^^^";TEZ,ZLOAD/(PI*RM^2)
2220 LPRINT "Z,R,T FIBER STRESSES=";
2230 LPRINT USING " ##.##^^^^";RSZF,RSRF,RSTF
2240 LPRINT "Z,R,T MATRIX STRESSES=";
2250 LPRINT USING " ##.##^^^^";RSZM(3),RSRM(3),RSTM(3)
2260 GOTO 250
2270 REM OUTPUT RESIDUAL STRESS DISTRIBUTION
2280 OPEN "O",#1,"RESID"
2290 FOR I=1 TO 5
2300 PRINT #1,RSZM(I),RSRM(I),RSTM(I)
2310 NEXT I
2320 PRINT #1,RSZF,RSRF,RSTF,TEZ,TEMP,TIM,HO
2330 CLOSE #1
2340 INPUT "ENTER 1 TO PRINT STRESSES ELSE 0";DUM9
2350 IF DUM9=0 THEN GOTO 2490
2360 LPRINT "  "
2370 LPRINT "TIME, TEMP, STRAIN, STRESS=";
2380 LPRINT USING " ##.##^^^^";TIM;TEMP;TEZ;ZLOAD/(PI*RM^2)
2390 LPRINT "  "
2400 LPRINT "FIBER STRESSES(Z,R,T)=";
2410 LPRINT USING " ###.## ";RSZF;RSRF;RSTF
2420 LPRINT "  "
2430 LPRINT "MATRIX STRESSES(Z,R,T)"
2440 FOR I=1 TO 5
2450 LPRINT "RADIAL POSITION=";RP(I)
2460 LPRINT USING " ###.## ";RSZM(I);RSRM(I);RSTM(I)
2470 NEXT I
2480 LPRINT "  "
2490 END
```

```
10 REM MECHANICAL/RELAXATION CONCENTRIC CYLINDER MODEL (MCCM)
20 REM INPUT RESIDUAL STRESS DISTRIBUTION
30 OPEN "I",#1,"RESID"
40 FOR I=1 TO 5
50 INPUT #1,RSZM(I),RSRM(I),RSTM(I)
60 NEXT I
70 INPUT #1,RSZF,RSRF,RSTF,TEZ,TEMP,TIM,HO
80 CLOSE #1
90 PRINT "TEMPERATURE(F) IS";TEMP
100 REM INPUT PROPERTIES OF FIBER(F) AND MATRIX(M)
110 REM ELASTIC CONSTANTS
120 EF=50000!:EM=11000!:VF=.25:VM=.35
130 REM RADIAL LOCATION OF BOUNDARIES
140 RF=.57:RM=1!
150 RP(1)=RF
160 RP(2)=.7
170 RP(3)=.82
180 RP(4)=.91
190 RP(5)=RM
200 INPUT "CYCLE, INITIAL STRAIN";CYC,TEZO
210 LPRINT "CYCLE";CYC
220 REM APPLIED AXIAL STRAIN EZ
230 INPUT "EZ AS +/-0.001 OR 0 TO TERMINATE";EZ
240 IF EZ=0 THEN GOTO 2020
250 REM GENERATE SYSTEM OF EQUATIONS FOR AN APPLIED STRAIN [A]x[X]=[B]
260 REM UNKNOWNS [X] ARE C1F, C1M, AND C2M (C2F=0)
270 REM WHERE THE RADIAL DISPLACEMENT U=C1*R+C2/R^2
280 REM STIFFNESS CONSTANTS FOR PLANE STRAIN (EZ IS CONSTANT)
290 REM CHECK FOR FLOW IN MATRIX
300 EFS=(RSZM(3)-RSRM(3))^2+(RSRM(3)-RSTM(3))^2
310 EFS=.707*(EFS+(RSTM(3)-RSZM(3))^2)^.5
320 YS=65!+HO
330 IF EFS<YS THEN FLOW=0:PRINT "EFS, YS=";EFS;YS:GOTO 400
340 PRINT "MATRIX FLOW DETECTED! EFS, YS=";EFS;YS
350 REM FLOW=0 ELASTIC BEHAVIOR
360 REM FLOW=1 ELASTIC BEHAVIOR WITH PRIOR HARDENING
370 REM FLOW=2 PLASTIC BEAHVIOR WITH PRIOR HARDENING
380 INPUT "FLOW(0=E 1=E&H 2=P&H), EZ";FLOW,EZ
390 IF FLOW>0 THEN HO=HO+EFS-YS
400 REM CALCULATE MATRIX STIFFNESS CONSTANTS AEM & AVM
410 IF FLOW=2 THEN AEM=2300:AVM=.49
420 IF FLOW<2 THEN AEM=EM:AVM=VM
430 PRINT "AEM, AVM=";AEM,AVM
440 K1F=EF*(1-VF)/((1+VF)*(1-2*VF))
450 K1M=AEM*(1-AVM)/((1+AVM)*(1-2*AVM))
460 K2F=VF*K1F/(1-VF)
470 K2M=AVM*K1M/(1-AVM)
480 REM GENERATE [A] MATRIX
490 REM UM=UF AT R=RF IS THE BASIS OF EQUATION 1
500 A(1,1)=RF
```

```
510 A(1,2)=-RF
520 A(1,3)=-1/RF
530 REM THE RADIAL STRESS SRM=0 AT R=RM IS THE BASIS OF EQUATION 2
540 A(2,1)=0
550 A(2,2)=K1M+K2M
560 A(2,3)=(K2M-K1M)/RM^2
570 REM SRM=SRF AT R=RF IS THE BASIS OF EQUATION 3
580 A(3,1)=-K1F-K2F
590 A(3,2)=K1M+K2M
600 A(3,3)=(K2M-K1M)/RF^2
610 REM GENERATE [B] MATRIX
620 B(1)=0
630 B(2)=-K2M*EZ
640 B(3)=(K2F-K2M)*EZ
650 REM TRIANGULARIZE SYSTEM OF LINEAR EQUATIONS
660 FOR I=1 TO 2
670 FOR J=I+1 TO 3
680 XX=A(J,I)/A(I,I)
690 FOR K=I+1 TO 3
700 A(J,K)=A(J,K)-A(I,K)*XX
710 NEXT K
720 B(J)=B(J)-B(I)*XX
730 NEXT J
740 NEXT I
750 REM SOLVE BY BACKWARD SUBSTITUTION
760 X(3)=B(3)/A(3,3)
770 FOR I=2 TO 1 STEP -1
780 DUM=0
790 FOR J=I+1 TO 3
800 DUM=DUM+A(I,J)*X(J)
810 NEXT J
820 X(I)=(B(I)-DUM)/A(I,I)
830 NEXT I
840 REM CALCULATE STRESSES(Si,j) AND STRAINS(Ei,j)
850 REM WHERE i IS A PRINCIPAL DIRECTION AND j IS A COMPONENT
860 REM ER=C1-C2/R^2 AND ET=U/R=C1+C2/R^2
870 C1F=X(1)
880 C1M=X(2)
890 C2M=X(3)
900 REM CALCULATE MATRIX STRAINS AND STRESSES
910 FOR I=1 TO 5
920 R=RP(I)
930 ERM=C1M-C2M/R^2
940 ETM=C1M+C2M/R^2
950 EZM=EZ
960 SRM=K1M*ERM+K2M*ETM+K2M*EZM
970 STM=K1M*ETM+K2M*ERM+K2M*EZM
980 SZM=K1M*EZM+K2M*ERM+K2M*ETM
990 RSZM(I)=RSZM(I)+SZM
1000 RSRM(I)=RSRM(I)+SRM
```

```
1010 RSTM(I)=RSTM(I)+STM
1020 PRINT "SZ, SR, ST ARE AT R=";
1030 PRINT USING "#.##";R
1040 PRINT USING " ##.##^^^^";RSZM(I),RSRM(I),RSTM(I)
1050 NEXT I
1060 REM CALCULATE FIBER STRAINS AND STRESSES
1070 R=RF
1080 ERF=C1F
1090 ETF=C1F
1100 EZF=EZ
1110 SRF=K1F*ERF+K2F*ETF+K2F*EZF
1120 STF=K1F*ETF+K2F*ERF+K2F*EZF
1130 SZF=K1F*EZF+K2F*ERF+K2F*ETF
1140 RSZF=RSZF+SZF
1150 RSRF=RSRF+SRF
1160 RSTF=RSTF+STF
1170 TEZ=TEZ+EZ
1180 PRINT "SZ, SR, ST IN FIBER"
1190 PRINT USING " ##.##^^^^";RSZF,RSRF,RSTF
1200 REM OUTPUT TEMPERATURE, STRAIN, AND STRESS
1210 PI=3.14159
1220 ZLOAD=PI*RF^2*RSZF
1230 FOR I=1 TO 4
1240 AVGS=(RSZM(I)+RSZM(I+1))/2
1250 AVGL=AVGS*PI*(RP(I+1)^2-RP(I)^2)
1260 ZLOAD=ZLOAD+AVGL
1270 NEXT I
1280 PRINT "COMPOSITE TEMPERATURE, STRAIN, AND STRESS"
1290 PRINT TEMP;
1300 PRINT USING " ##.##^^^^";TEZ,ZLOAD/(PI*RM^2)
1310 REM RELAX STRESSES
1320 REM CALCULATE EXTERNAL LOAD
1330 PI=3.14159
1340 ELOAD=PI*RF^2*RSZF
1350 FOR I=1 TO 4
1360 AVGS=(RSZM(I)+RSZM(I+1))/2
1370 AVGL=AVGS*PI*(RP(I+1)^2-RP(I)^2)
1380 ELOAD=ELOAD+AVGL
1390 NEXT I
1400 REM INPUT TIME INCREMENT(TI SET FOR 0.001 PER SECOND)
1410 TI=1000*ABS(EZ)
1420 TIM=TIM+TI
1430 REM ADJUST MATRIX STRESSES
1440 FOR I=1 TO 5
1450 S=RSZM(I)
1460 GOSUB 1740
1470 RSZM(I)=S
1480 S=RSRM(I)
1490 GOSUB 1740
1500 RSRM(I)=S
```

```
1510 S=RSTM(I)
1520 GOSUB 1740
1530 RSTM(I)=S
1540 NEXT I
1550 REM ADJUST TRANSVERSE FIBER STRESSES
1560 RSRFO=RSRF
1570 RSRF=RSRM(1)
1580 RSTF=RSRF
1590 REM CALCULATE LOAD CARRIED BY FIBER
1600 MLOAD=0
1610 FOR I=1 TO 4
1620 AVGS=(RSZM(I)+RSZM(I+1))/2
1630 AVGL=AVGS*PI*(RP(I+1)^2-RP(I)^2)
1640 MLOAD=MLOAD+AVGL
1650 NEXT I
1660 FLOAD=ELOAD-MLOAD
1670 RSZFO=RSZF
1680 REM ADJUST Z STRESS OF FIBER
1690 RSZF=FLOAD/(PI*RF^2)
1700 REM CALCULATE COMPOSITE STRAIN
1710 EZ=((RSZF-RSZFO)-2*VF*(RSRF-RSRFO))/EF
1720 TEZ=TEZ+EZ
1730 GOTO 1790
1740 REM RELAXATION SUBROUTINE
1750 IF ABS(S)>26.5 THEN DS=ABS(S)/50 ELSE DS=3.76E-07*ABS(S)^4.32
1760 IF S<0 THEN DS=-DS
1770 S=S-DS*TI
1780 RETURN
1790 REM OUTPUT STRESSES, TEMPERATURE, AND AXIAL STRAIN
1800 FOR I=1 TO 5
1810 PRINT "SZ, SR, ST ARE AT R=";
1820 PRINT USING "#.##";R(I)
1830 PRINT USING " ##.##^^^^";RSZM(I),RSRM(I),RSTM(I)
1840 NEXT I
1850 PRINT "SZ, SR, ST IN FIBER"
1860 PRINT USING " ##.##^^^^";RSZF,RSRF,RSTF
1870 PRINT "COMPOSITE TEMPERATURE, STRAIN, AND STRESS"
1880 PRINT TEMP;
1890 PRINT USING " ##.##^^^^";TEZ,ELOAD/(PI*RM^2)
1940 LPRINT "TIME, TEMP, STRAIN, STRESS"
1950 LPRINT USING " ##.##^^^^";TIM,TEMP,TEZ,ELOAD/(PI*RM^2)
1960 LPRINT "FIBER STRESSES(Z,R,T)"
1970 LPRINT USING " ###.## ";RSZF,RSRF,RSTF
1980 LPRINT "MATRIX STRESSES(Z,R,T)"
1990 FOR I=1 TO 5
2000 LPRINT USING " ###.## ";RSZM(I),RSRM(I),RSTM(I)
```

```
2010 NEXT I
2011 LPRINT "EFS, YS, AEM, STRAIN=";
2012 LPRINT USING " ##.##^^^^";EFS,YS,AEM,TEZ-TEZO
2015 GOTO 230
2020 OPEN "O",#1,"RESID"
2030 FOR I=1 TO 5
2040 PRINT #1,RSZM(I),RSRM(I),RSTM(I)
2050 NEXT I
2060 PRINT #1,RSZF,RSRF,RSTF,TEZ,TEMP,TIM,HO
2070 CLOSE #1
2080 END
```

TABLE I. - FATIGUE TEST RESULTS OF THE Ti-15-3 MATRIX ALLOY

Temperature, °C	Strain range, $\Delta\varepsilon$ - percent	Cycle 1		Cycle 100		Cycle $0.5N_f$		Fatigue life, cycles
		Stress range, $\Delta\sigma$ - MPa	Mean stress, σ_m - MPa	Stress range, $\Delta\sigma$ - MPa	Mean stress, σ_m - MPa	Stress range, $\Delta\sigma$ - MPa	Mean stress, σ_m - MPa	
300	0.428	401	201	394	197	380	200	254 104[a]
↓	.464	441	221	418	219	431	216	161 000[a]
	.606	558	277	570	261	570	285	9 488
	.850	786	330	781	320	774	326	4 274
550	.578	447	210	462	56	476	9	201 793[a]
550	.682	534	211	542	53	546	17	13 728
550	.785	648	228	613	52	607	9	16 500

[a]Failure in threads.

TABLE II. - FATIGUE TEST RESULTS OF THE SiC/Ti-15-3 COMPOSITE

Temperature, °C	Stress range, $\Delta\sigma$ - MPa	Cycle 1		Cycle 100		Cycle $0.5N_f$		Fatigue life, N_f - cycles
		Strain range, $\Delta\varepsilon$ - percent	Mean strain, ε_m - percent	Strain range, $\Delta\varepsilon$ - percent	Mean strain, ε_m - percent	Strain range, $\Delta\varepsilon$ - percent	Mean strain, ε_m - percent	
300	757	0.428	0.214	0.433	0.220	0.427	0.168	50 930
↓	879	.492	.246	.490	.252	.484	.229	16 076
	1103	.654	.327	.650	.329	.658	.330	3 375
	1278	.812	.406	.826	.463	.828	.484	904
550	656	.398	.199	.408	.249	.406	.318	68 299
↓	758	.470	.235	.468	.310	.464	.330	13 817
	974	.552	.276	.539	.373	.566	.443	2 810
	1078	.626	.313	-----	-----	.632	.413	42
	1095	.636	.318	-----	-----	.644	.385	10

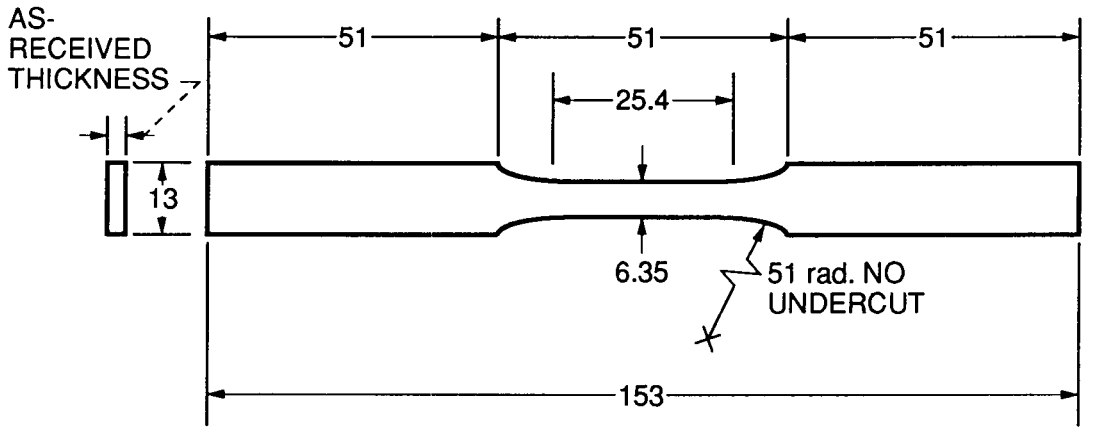

Figure 1. - SiC/Ti-15-3 composite test specimen. (All dimensions are in mm.)

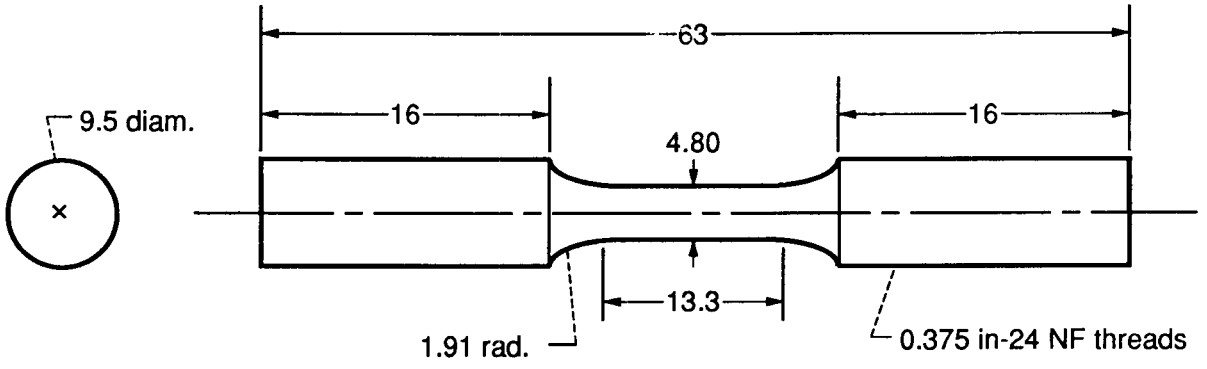

Figure 2. - Ti-15-3 matrix alloy test specimen. (All dimensions are in mm.)

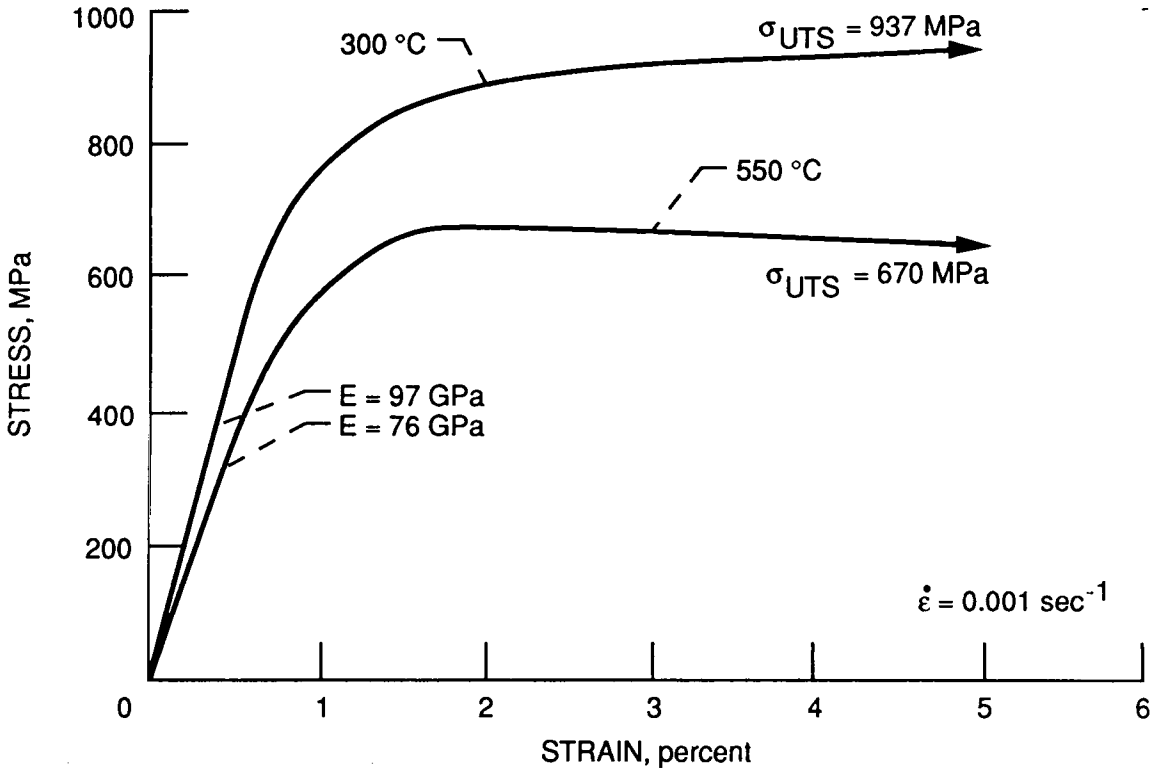

Figure 3. - Ti-15-3 matrix alloy tensile data.

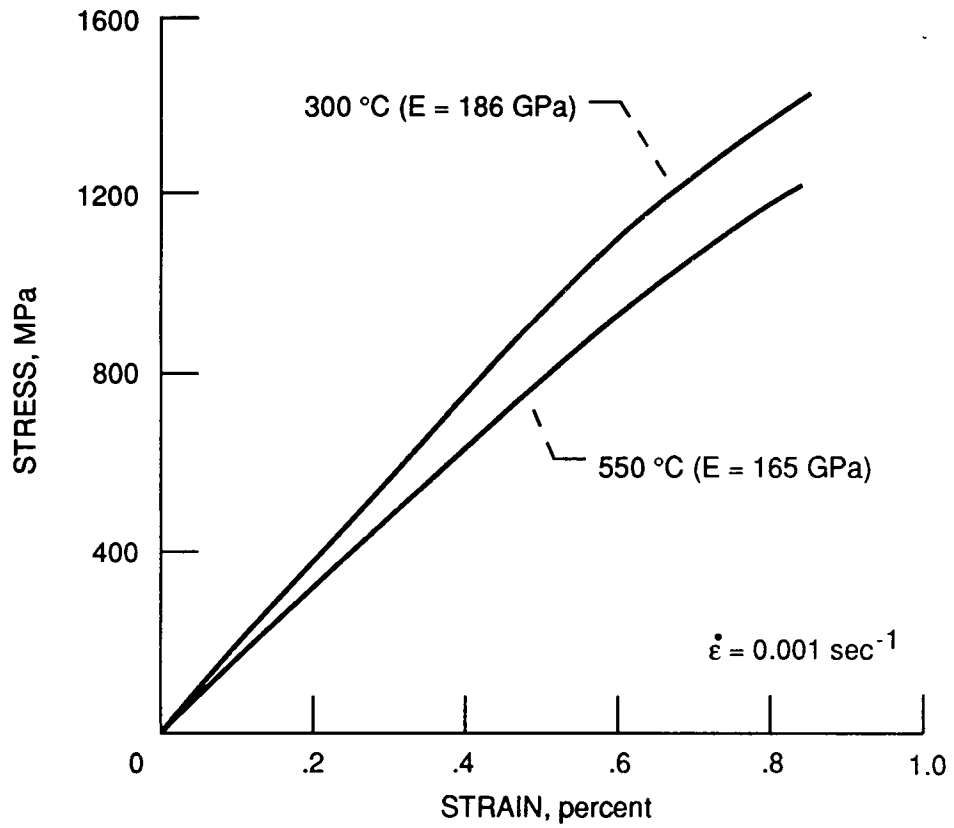

Figure 4. - SiC/Ti-15-3 composite tensile data.

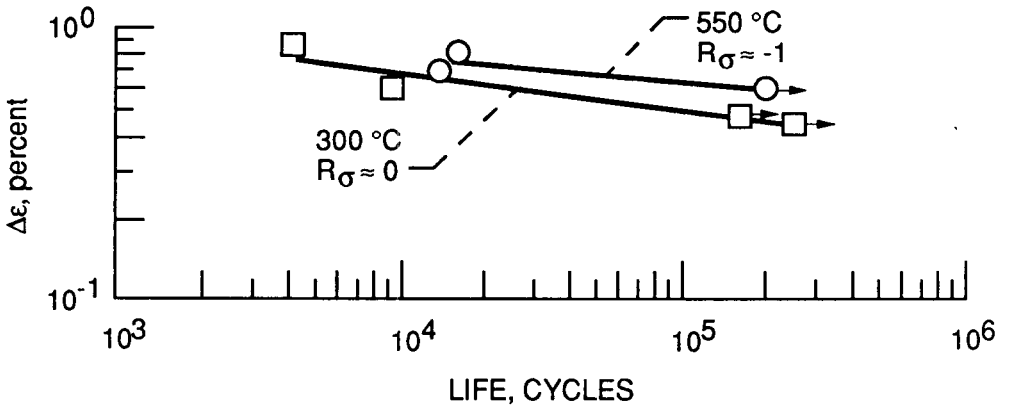

Figure 5. - Strain-controlled isothermal fatigue life of the Ti-15-3 matrix alloy.

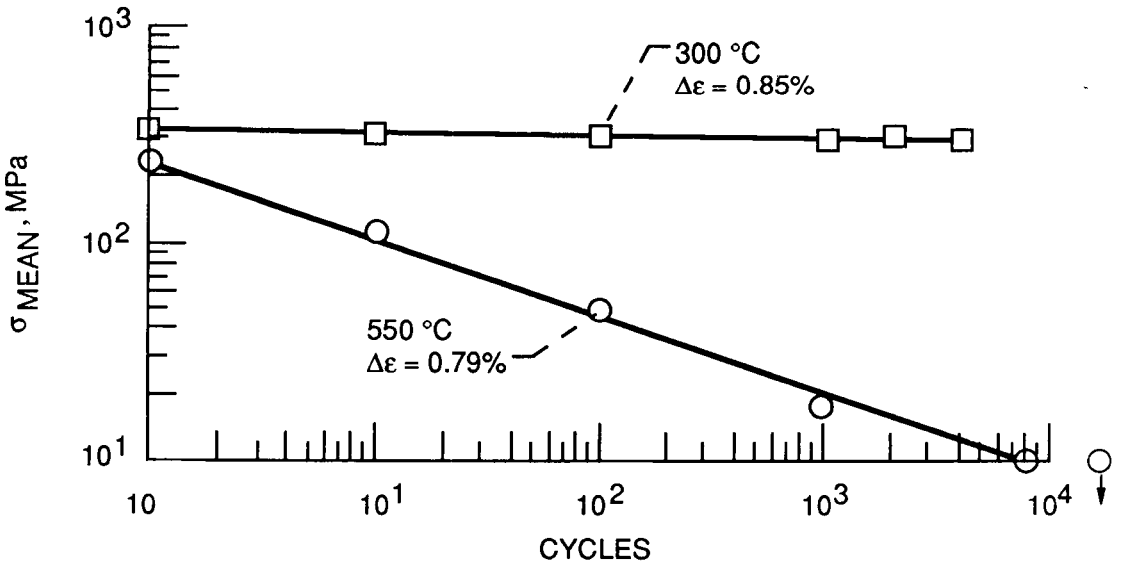

Figure 6. - Observed change in mean stress during isothermal fatigue testing of the Ti-15-3 matrix alloy.

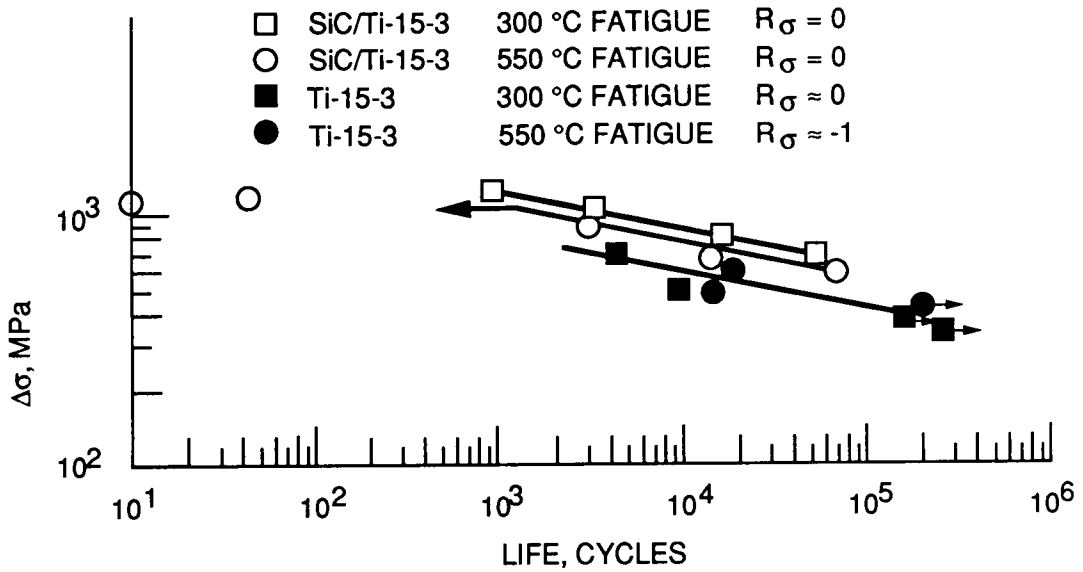

Figure 7. - Stress-based comparison of isothermal fatigue life of SiC/Ti-15-3 composite (load-controlled) and the Ti-15-3 matrix alloy (strain-controlled).

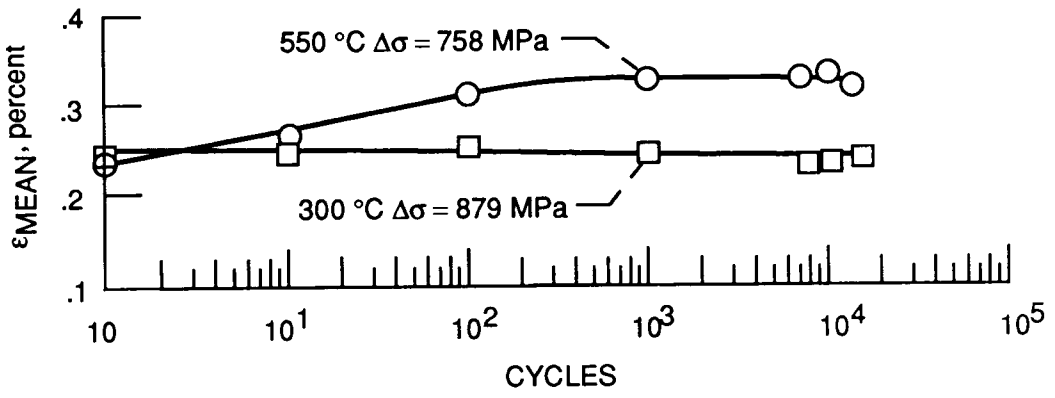

Figure 8. - Observed change in mean strain during isothermal fatigue test of SiC/Ti-15-3 composite.

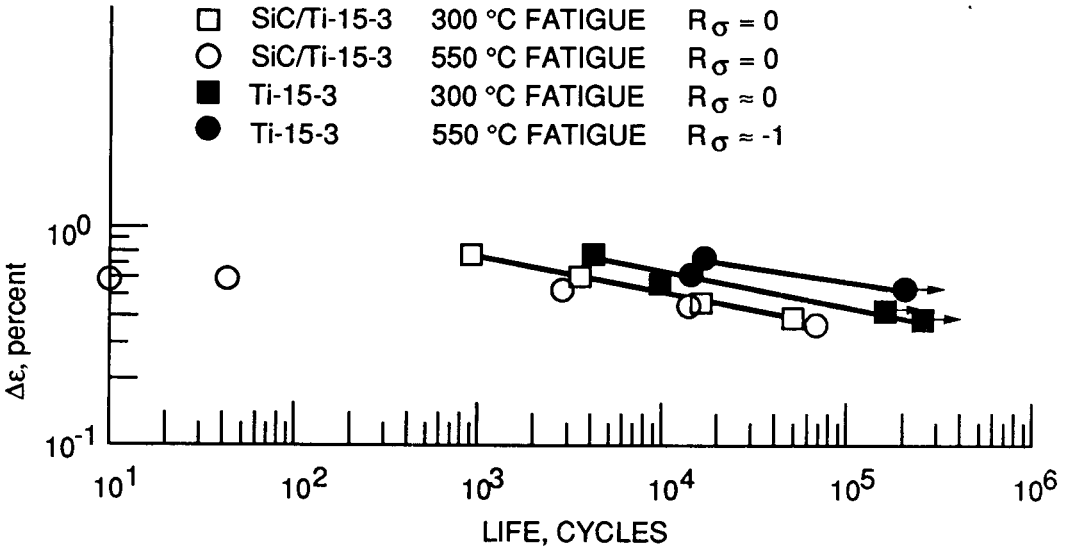

Figure 9. - Strain-based comparison of the isothermal fatigue life of SiC/Ti-15-3 composite (load-controlled) and the Ti-15-3 matrix alloy (strain-controlled).

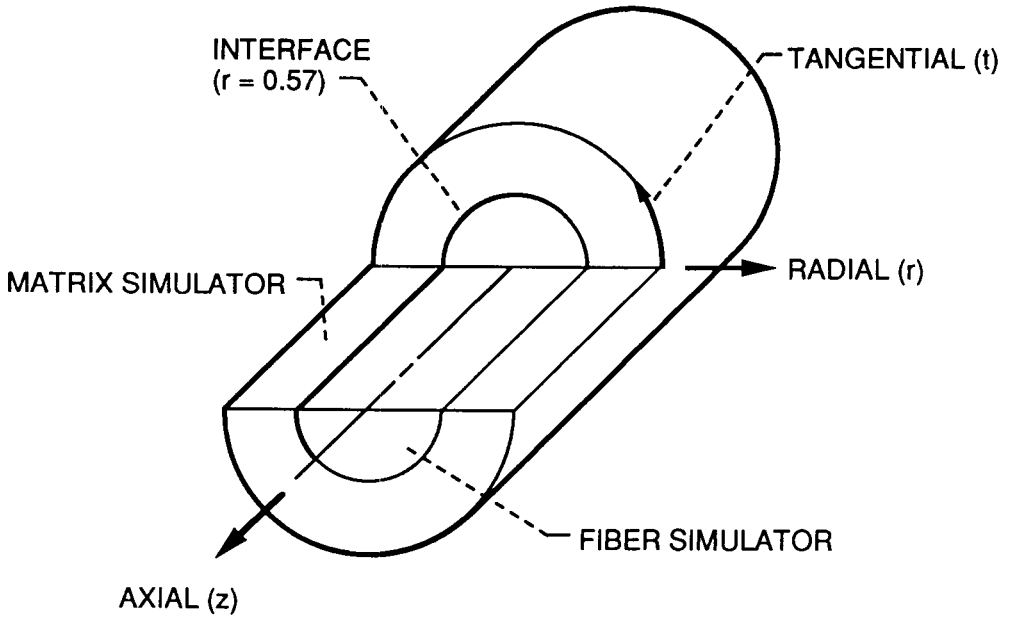

Figure 10. - Cutaway of composite simulator for 33% volume fraction. Note that z, r, and t are the principal stress directions.

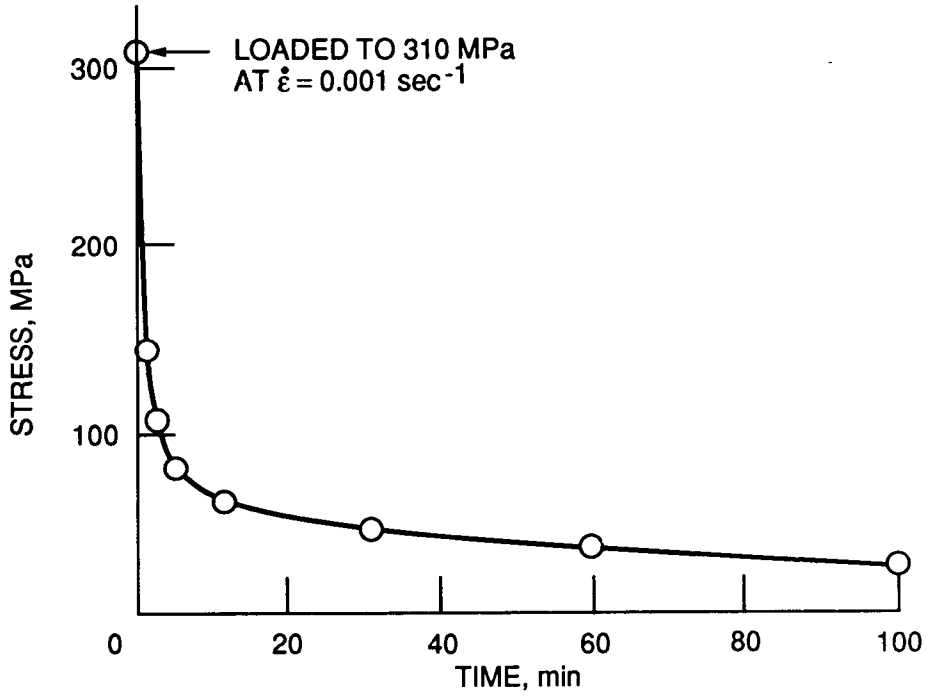

Figure 11. - Stress relaxation behavior of the Ti-15-3 matrix alloy at 550 °C.

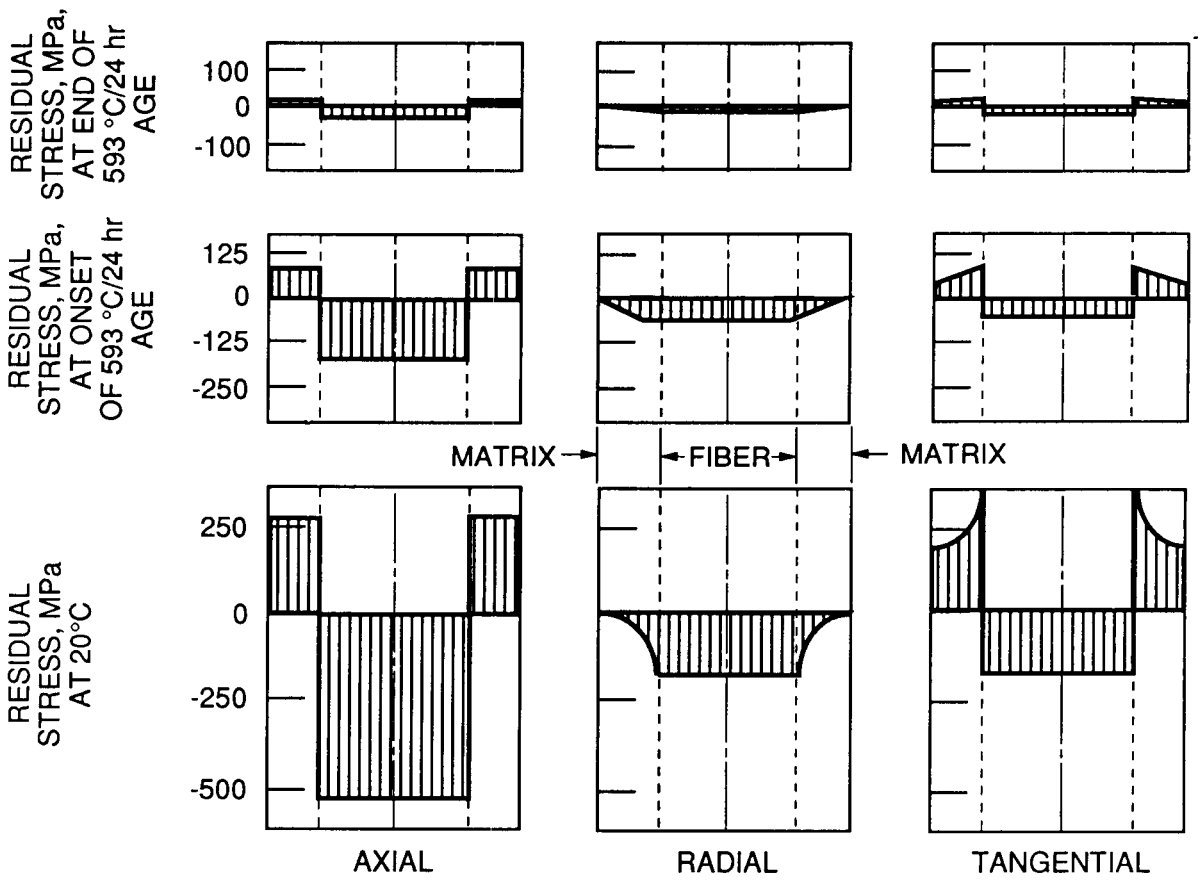

Figure 12. - Thermally generated residual stress distributions in the composite at 20 °C, at the onset of the 593 °C age, and at the end of the 593 °C age.

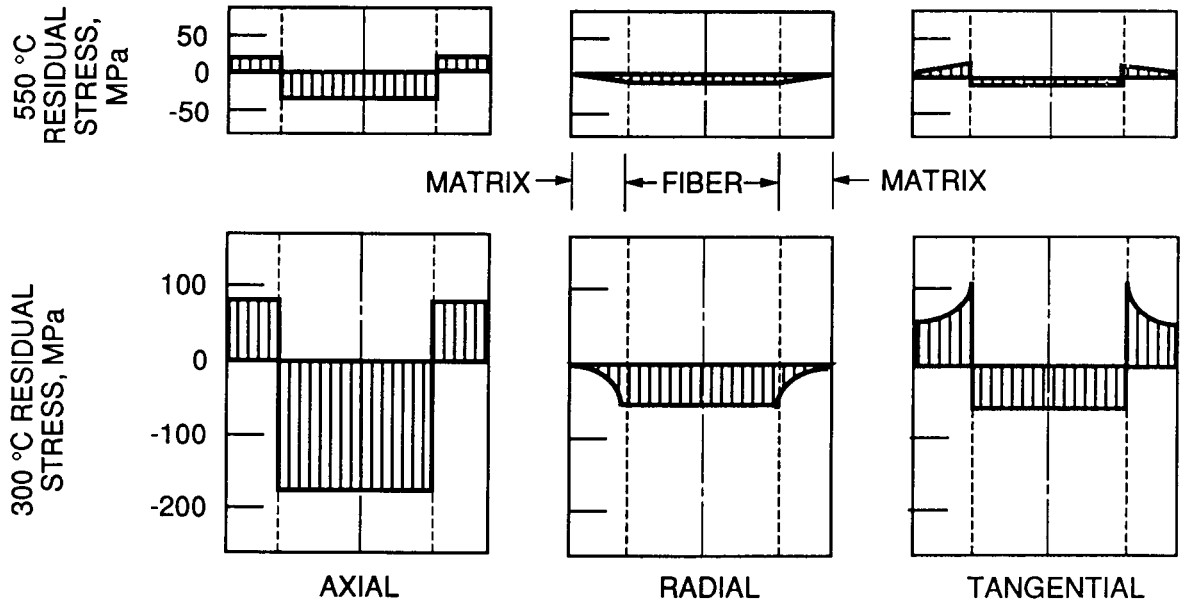

Figure 13. - Thermally generated residual stress distributions in composite at 300 and 550 °C.

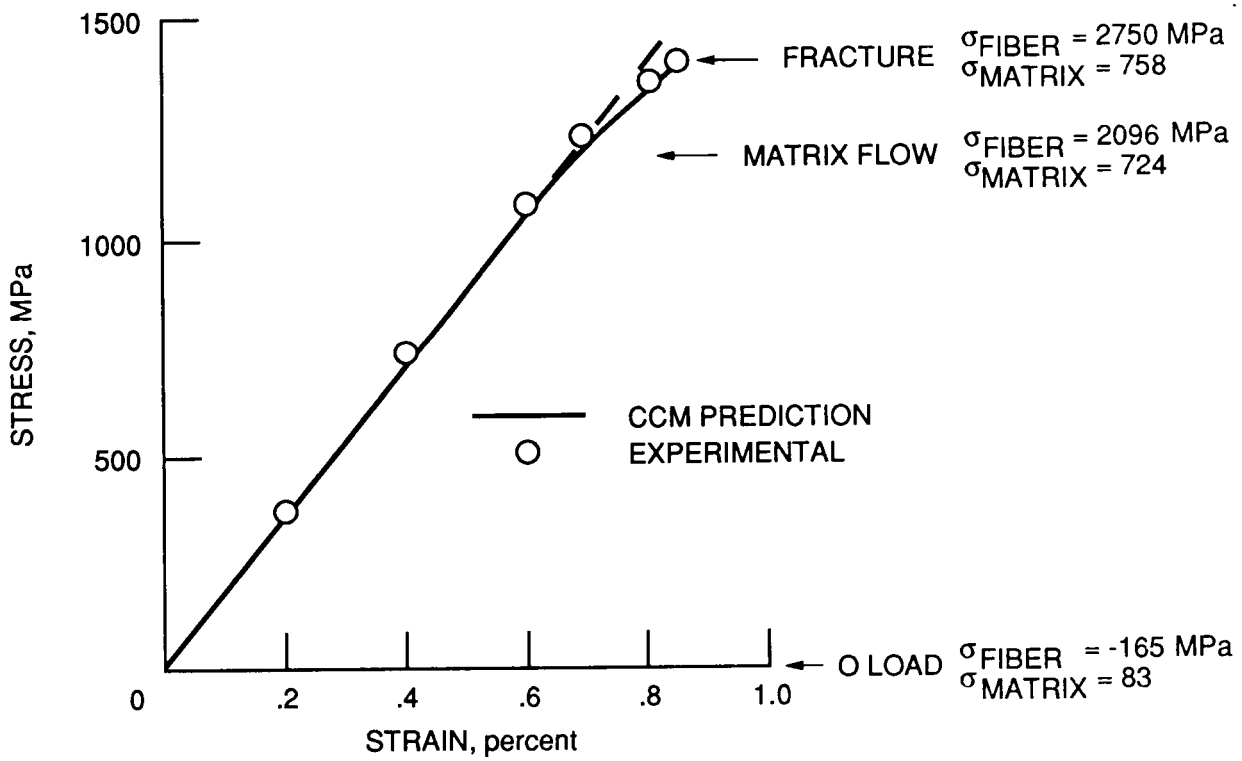

Figure 14. - Predicted tensile behavior of the composite at 300 °C.

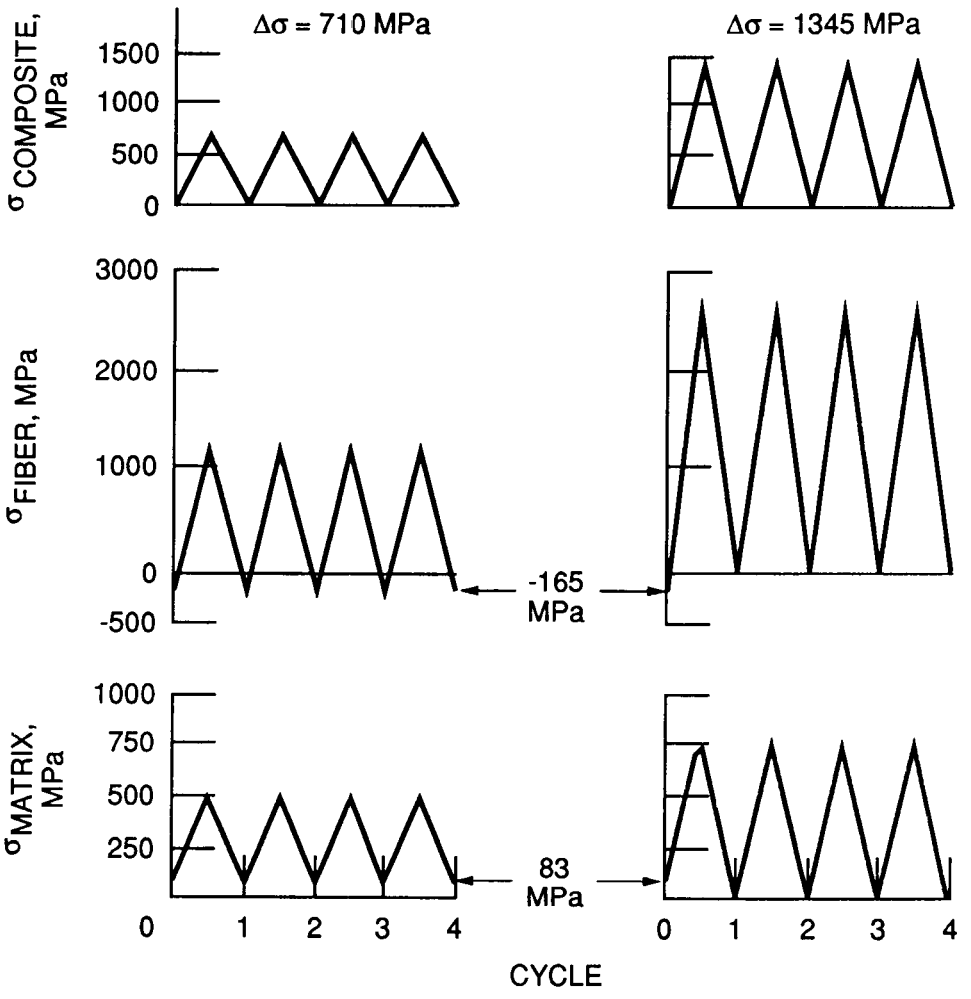

Figure 15. - Variation in axial stress of the composite, fiber, and matrix during 300 °C isothermal fatigue tests.

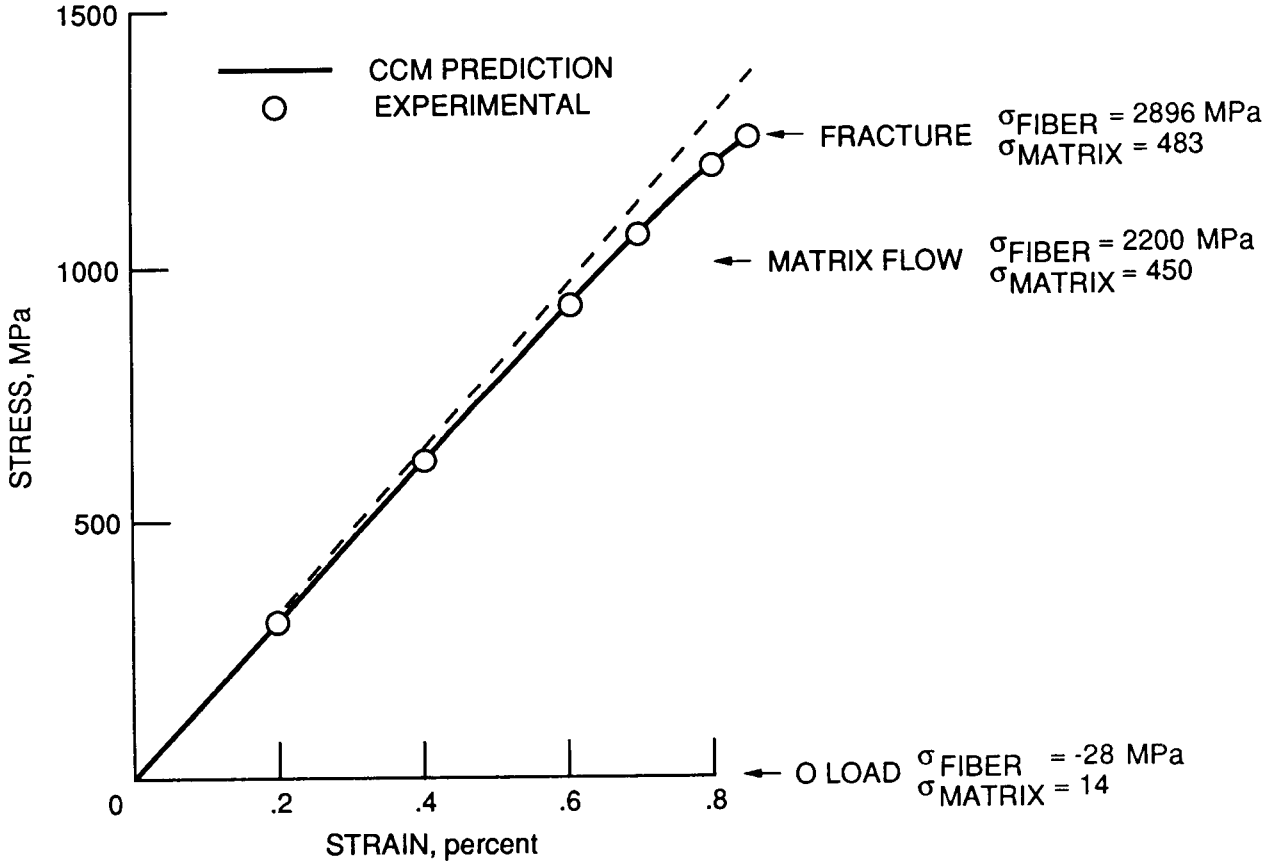

Figure 16. - Predicted tensile behavior of composite at 550 °C.

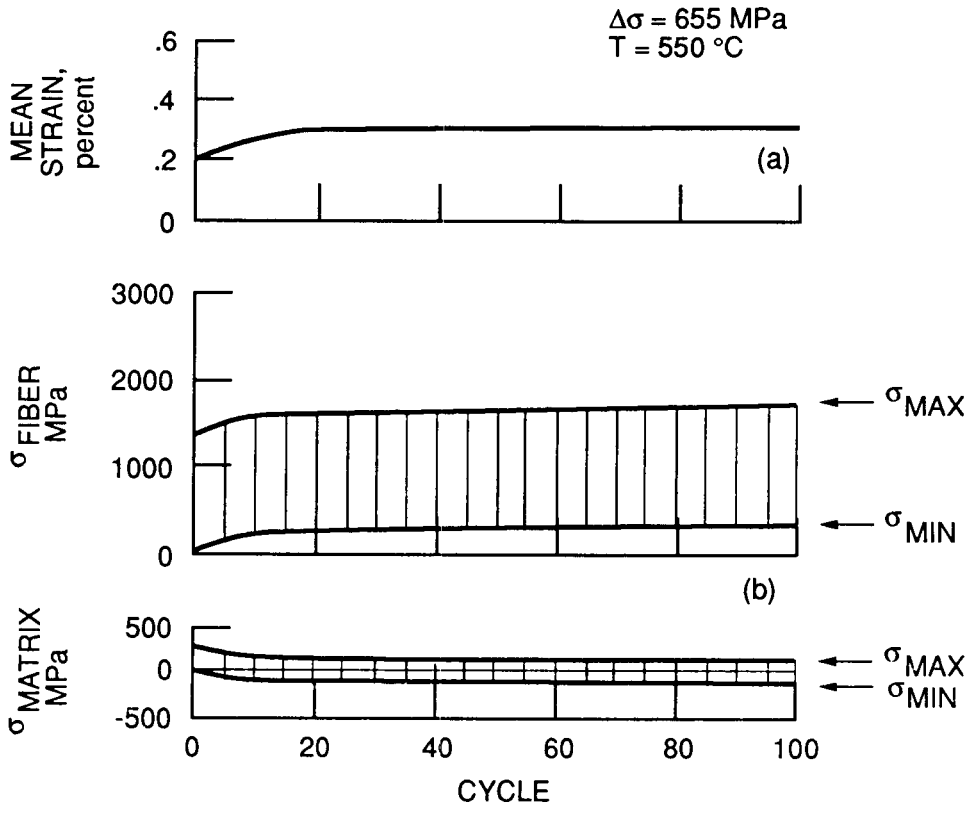

Figure 17. - Predicted change in mean strain (a), fiber and matrix stress (b) during a 550 °C isothermal fatigue test on the SiC/Ti composite. Low stress range, $\Delta\sigma$ = 655 MPa.

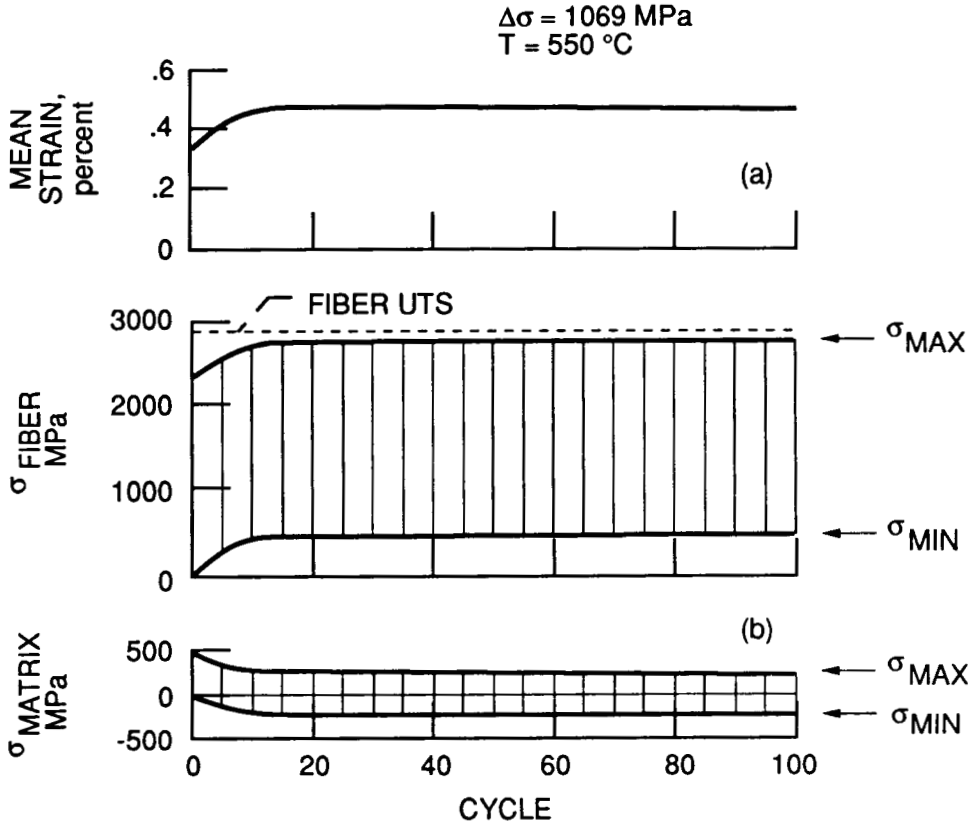

Figure 18. - Predicted change in mean strain (a), fiber and matrix stress (b) during a 550 °C isothermal fatigue test on the SiC/Ti composite. High stress range, $\Delta\sigma$ = 1069 MPa.

NASA
National Aeronautics and Space Administration

Report Documentation Page

1. Report No.	2. Government Accession No.	3. Recipient's Catalog No.
NASA TM-101984		

4. Title and Subtitle	5. Report Date
The Isothermal Fatigue Behavior of a Unidirectional SiC/Ti Composite and the Ti Alloy Matrix	April 1989
	6. Performing Organization Code

7. Author(s)	8. Performing Organization Report No.
John Gayda, Jr., Timothy P. Gabb, and Alan D. Freed	E-4683
	10. Work Unit No. 505-63-1A

9. Performing Organization Name and Address	11. Contract or Grant No.
National Aeronautics and Space Administration Lewis Research Center Cleveland, Ohio 44135-3191	
	13. Type of Report and Period Covered Technical Memorandum

12. Sponsoring Agency Name and Address	14. Sponsoring Agency Code
National Aeronautics and Space Administration Washington, D.C. 20546-0001	

15. Supplementary Notes

16. Abstract

The high temperature fatigue behavior of a metal matrix composite (MMC) consisting of Ti-15V-3Cr-3Al-3Sn (Ti-15-3) matrix reinforced by 33 vol % of continuous unidirectional SiC fibers was experimentally and analytically evaluated. Isothermal MMC fatigue tests with constant amplitude loading parallel to the fiber direction were performed at 300 and 550 °C. Comparative fatigue tests of the Ti-15-3 matrix alloy were also conducted. Composite fatigue behavior and the in-situ stress state of the fiber and matrix were analyzed with a micromechanical model, the Concentric Cylinder Model (CCM). The cyclic stress-strain response of the composite was stable at 300 °C. However, an increase in cyclic mean strain foreshortened MMC fatigue life at high strain ranges at 550 °C. Fatigue tests of the matrix alloy and CCM analyses indicated this response was associated with stress relaxation of the matrix in the composite.

17. Key Words (Suggested by Author(s))	18. Distribution Statement
Fatigue Composite	Unclassified – Unlimited Subject Category 24

19. Security Classif. (of this report)	20. Security Classif. (of this page)	21. No of pages	22. Price*
Unclassified	Unclassified	36	A03

*For sale by the National Technical Information Service, Springfield, Virginia 22161